Spirals and secondary instabilities in the Taylor-Couette flow.

J. Antonijoan[1] F. Marquès[2] J. Sánchez[2]

Abstract

The spiral flow is the first bifurcation of the basic flow that appears between counter-rotating cylinders, and small increases of the Reynolds number give rise to a variety of secondary flows including interpenetrating spirals, turbulent bursts and others [1], [2]. In order to carry out a linear stability analysis of the spirals, the numerical computation of this flow for different parameter values is needed. In this work the spiral flow is computed numerically and its main features are described in detail. Some results on instabilities and bifurcations will also be presented.

1 The model.

The Couette apparatus is made of two concentric cylinders, of inner and outer radius r_i, r_o and gap $d = r_o - r_i$, that can rotate independently with frequencies Ω_i, Ω_o. The nondimensional parameters are the radius ratio $\eta = r_i/r_o$, and the Reynolds numbers associated with the rotation frequencies of the cylinders $R_i = dr_i\Omega_i/\nu$, $R_o = dr_o\Omega_o/\nu$ where ν is the kinematic viscosity. We will assume infinite cylinders, and solutions periodic in the axial direction of period $2\pi b$. We use cylindrical coordinates (r, θ, z) and we adimensionalize the equations using d, d^2/ν, $(\nu/d)^2$ for space, time, and pressure (in fact p/ρ_o with ρ_o the constant density of the fluid) respectively.

The spiral flow that appears in the counter rotating case has a spatial structure invariant with respect to a rotation around the cylinder's axis and a simultaneous translation in the axis direction, i.e. a helical movement that we will term a helical symmetry. This symmetry can be written in cylindrical coordinates

$$(r, \theta, z) \quad \longrightarrow \quad (r, \theta + \beta, z + b\beta) \tag{1}$$

where β is the rotation angle and $2\pi b$ is the axial period, a constant which fix the relative magnitude of the rotation and the translation. b is also related to the slope of the spiral pattern.

We are looking for velocity fields whose components are functions only of the radial coordinate r and the special combination ρ. These velocity fields are invariant with respect to helical symmetries. The three-dimensional structure of these flows is now described by using only two space coordinates, and the flow can be numerically computed in detail.

We introduce the mean velocities in the azimuthal and axial directions as averages over ρ and we use toroidal and poloidal potentials for the ρ-dependent velocity part.

$$\mathbf{v} = \overline{v}_\theta \hat{\mathbf{e}}_\theta + \overline{v}_z \hat{\mathbf{e}}_z + \nabla \times (\psi \hat{\mathbf{e}}_z) + \nabla \times \nabla \times (\phi \hat{\mathbf{e}}_z) \tag{2}$$

where

$$\overline{v}_\theta = P_\rho v_\theta, \quad \overline{v}_z = P_\rho v_z, \quad P_\rho F = \frac{1}{2\pi}\int_0^{2\pi} F(r, \rho, t) d\rho \tag{3}$$

The incompressibility condition is thus avoided, and the pressure is removed from the formulation. The equations for the mean velocities are the averaged θ and z components of the Navier-Stokes equations,

[1] Dept. Matemàtica i Telemàtica. Universitat Politècnica de Catalunya. Av. Víctor Balaguer s/n, E-08800 Vilanova i la Geltrú.

[2] Dept. Física Aplicada. Universitat Politècnica de Catalunya. c/ Gran Capità s/n, Mod. B5 Campus Nord, E-08034 Barcelona.

and we will use the axial components of the curl and double curl of the Navier–Stokes equations for the potentials.

$$(\partial_t - DD_+)\overline{v}_\theta = -P_\rho \hat{\mathbf{e}}_\theta \cdot \boldsymbol{\omega} \times \mathbf{v} \tag{4}$$
$$(\partial_t - D_+D)\overline{v}_z = -P_\rho \hat{\mathbf{e}}_z \cdot \boldsymbol{\omega} \times \mathbf{v} \tag{5}$$
$$(\partial_t - \Delta)\Delta_h \psi = (1 - P_\rho)\hat{\mathbf{e}}_z \cdot \nabla \times \boldsymbol{\omega} \times \mathbf{v} \tag{6}$$
$$(\partial_t - \Delta)\Delta\Delta_h \phi = -(1 - P_\rho)\hat{\mathbf{e}}_z \nabla \times \nabla \times \boldsymbol{\omega} \times \mathbf{v} \tag{7}$$

The corresponding boundary conditions are:

$$\begin{array}{c} \overline{v}_\theta(r_i) = R_i, \ \overline{v}_\theta(r_o) = R_o \\ \left.\begin{array}{l} \overline{v}_z = D\psi = \phi = \Delta_h \phi = 0 \\ -b\psi + rD\phi = b\Delta\Delta_h\phi + rD\Delta_h\psi = 0 \end{array}\right\} \text{ on } r = r_i, \ r_o \end{array} \tag{8}$$

The last boundary condition is necessary in order to ensure the equivalence with the Navier–Stokes equation. The velocity potentials are not uniquely determined by the velocity field, so we have used $\phi = 0$ as a gauge boundary condition. The remaining boundary conditions come from the no slip condition on the cylinders surface. More details on these conditions can be found in [3], [4]. Small omega is the vorticity and D is the radial derivative.

2 Numerical methods.

In order to solve these equations we have used spectral methods. The potentials have been expanded using Chebishev polynomials in the radial direction, and a Fourier expansion for the ρ coordinate.

$$\overline{v}_\theta(x) = \sum_{l=0}^{L} f_l T_l(x) \tag{9}$$
$$\psi(x, \rho) = \sum_{l=0}^{L} \sum_{\substack{n=-N/2 \\ n \neq 0}}^{N/2-1} \psi_{l,n} T_l(x) e^{in\rho} \tag{10}$$

and analogous developments for $\overline{v}_z$ and ϕ. $x = 2(r - r_i)/d - 1$ in order to ensure $x \in [-1, 1]$.

The spiral flow is periodic in time, the whole pattern rotating around the cylinders axis with angular velocity Ω. Therefore, in a rotating reference frame with frequency Ω we have a steady flow. The Navier–Stokes equations in the rotating frame include now the Coriolis term, which is equivalent to change $\boldsymbol{\omega}$ by $\boldsymbol{\omega} + 2\Omega\hat{\mathbf{e}}_z$, and the centrifugal term, which can be included in the pressure. The Reynolds numbers in the rotating frame changes into $R_i \to R_i - \Omega r_i$, $R_o \to R_o - \Omega r_o$.

Being now the spiral a fixed point, it can be computed using continuation methods, for different parameter values. Figure 1 shows a typical plot of the solutions obtained by continuation methods. We have plotted the value of a mode in a point versus the inner Reynolds number. The pinch at point b corresponds to the fact that in a small range of Reynolds number almost all modes change sign. But the branches do not touch each other. As we will see, secondary bifurcations take place near the point a. The results displayed from now on correspond to the parameter values $R_o = -50$, $\eta = 0.80$, $b = b_{\text{crit}} = 0.3055$. b_{crit} is the critical value on the transition to spirals, which take place for $R_i = 106.1$ in this case.

The bifurcation looks like a pitchfork as a result of working in the rotating frame where the spiral is at rest. The rotational symmetry gives a circle of stationary solutions which differ in a phase, and in order to fix this phase we have imposed the condition that the imaginary part of the dominant mode be zero. The real part can be positive or negative, giving the two symmetrical branches shown.

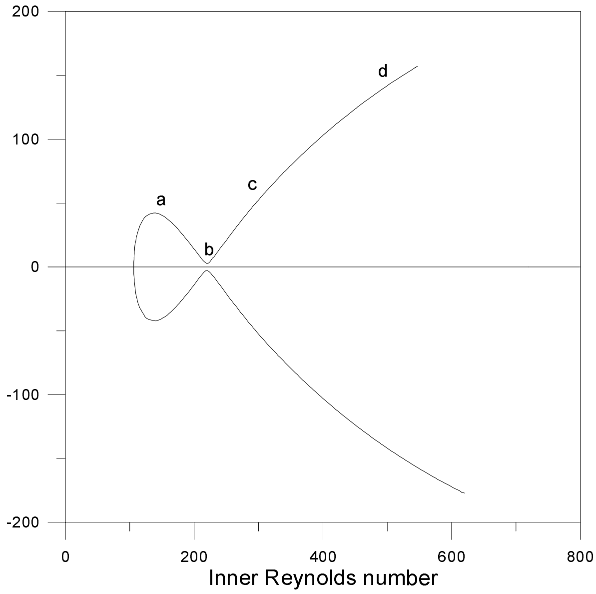

Figure 1: Branches of spiral flow obtained using continuation methods. The parameter values are given in the text.

3 Spiral flow properties.

Let us go to look into the properties of the spirals labeled a, b, c, d in the diagram. The behavior of the mean flows is displayed in Figure 2. We see that when we increase the Reynolds number, two boundary layers develop near the walls, and the fluid in the center of the cylinders has zero average azimuthal velocity –is at rest on the rotating system. But it has a slow average motion in the axial direction. This gives a large scale motion on the z axis. And a non zero net mass flux appears in the axial direction, showed in Figure 2d. This net flux changes sign when we increase the Reynolds number.

In Figure 3 we see the global structure of the flow. Figure 3a shows a perspective view of the velocity field for the mean radius. The flow looks sinusoidal near the transition, but for high Reynolds number the center of the vortices is almost at rest, as the mean flows also showed. This suggest that the core of the vortices tends to move like a rigid body, and in the rotating reference frame are at rest. This rigid body rotation is confirmed by the Figure 3d (isolines of vertical vorticity), which shows that the vertical vorticity in the center is constant (in fact zero).

Figure 3b shows the velocity field in a θ constant section. When the Reynolds number increases, we see the formation of a outgoing jet. Figure 3c shows the isolines of the azimuthal velocity, showing the formation of the aforementioned jet, which maintains the angular momentum up to collide with the outer wall. Near the walls and between the vortices, boundary layers appear.

These results are similar in many aspects to those obtained by Fasel and Booz in 1984 [5], for the Taylor Vortex Flow at high Reynolds numbers.

4 Stream function and trajectories.

The incompressibility condition written in the $(r,\, \rho)$ coordinates for the spiral flow is

$$\frac{1}{r}\partial_r(rv_r) + \partial_\rho\left(\frac{v_z}{b} - \frac{v_\theta}{r}\right) = 0 \tag{11}$$

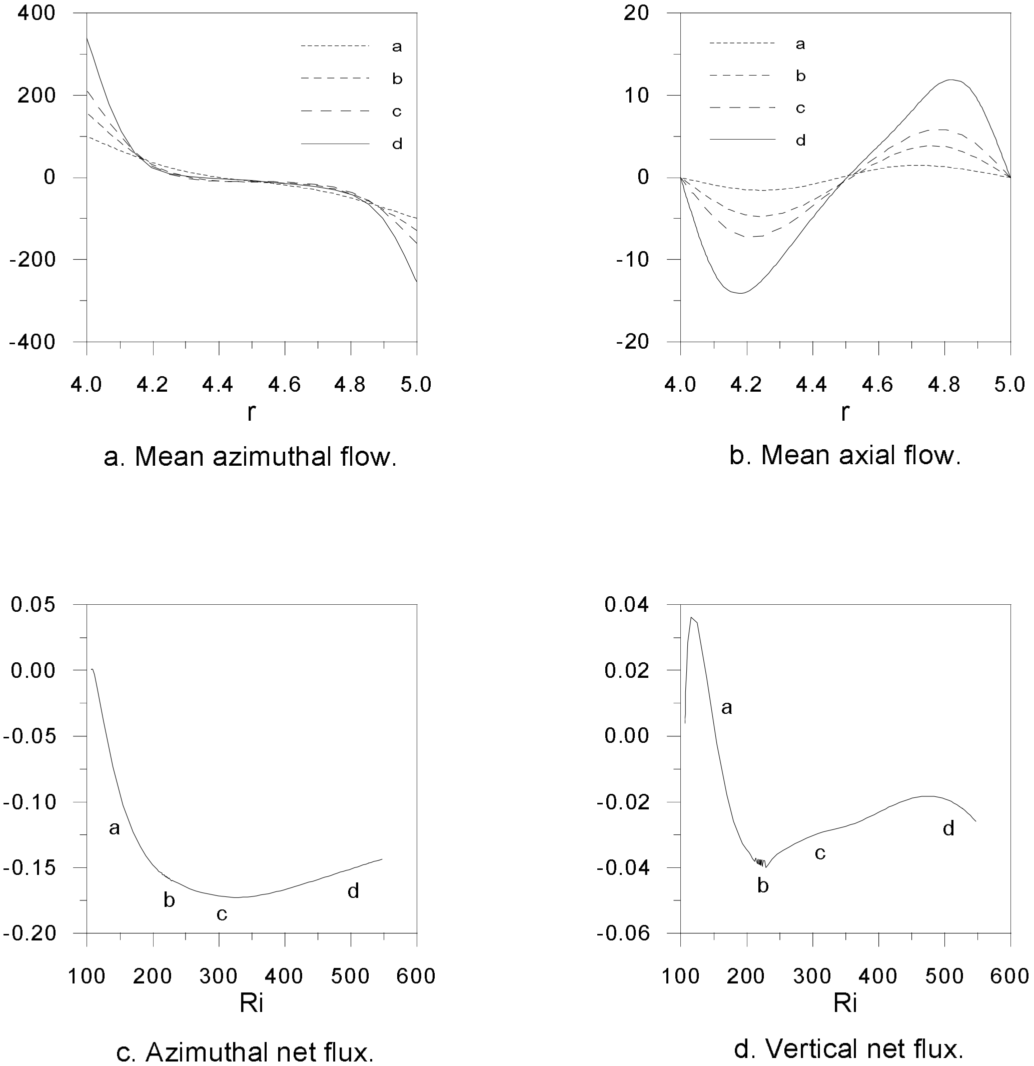

a. Mean azimuthal flow.

b. Mean axial flow.

c. Azimuthal net flux.

d. Vertical net flux.

Figure 2: a,b Mean flows. c,d net flun normalized with the net azimuthal flux of the basic Couette flow.

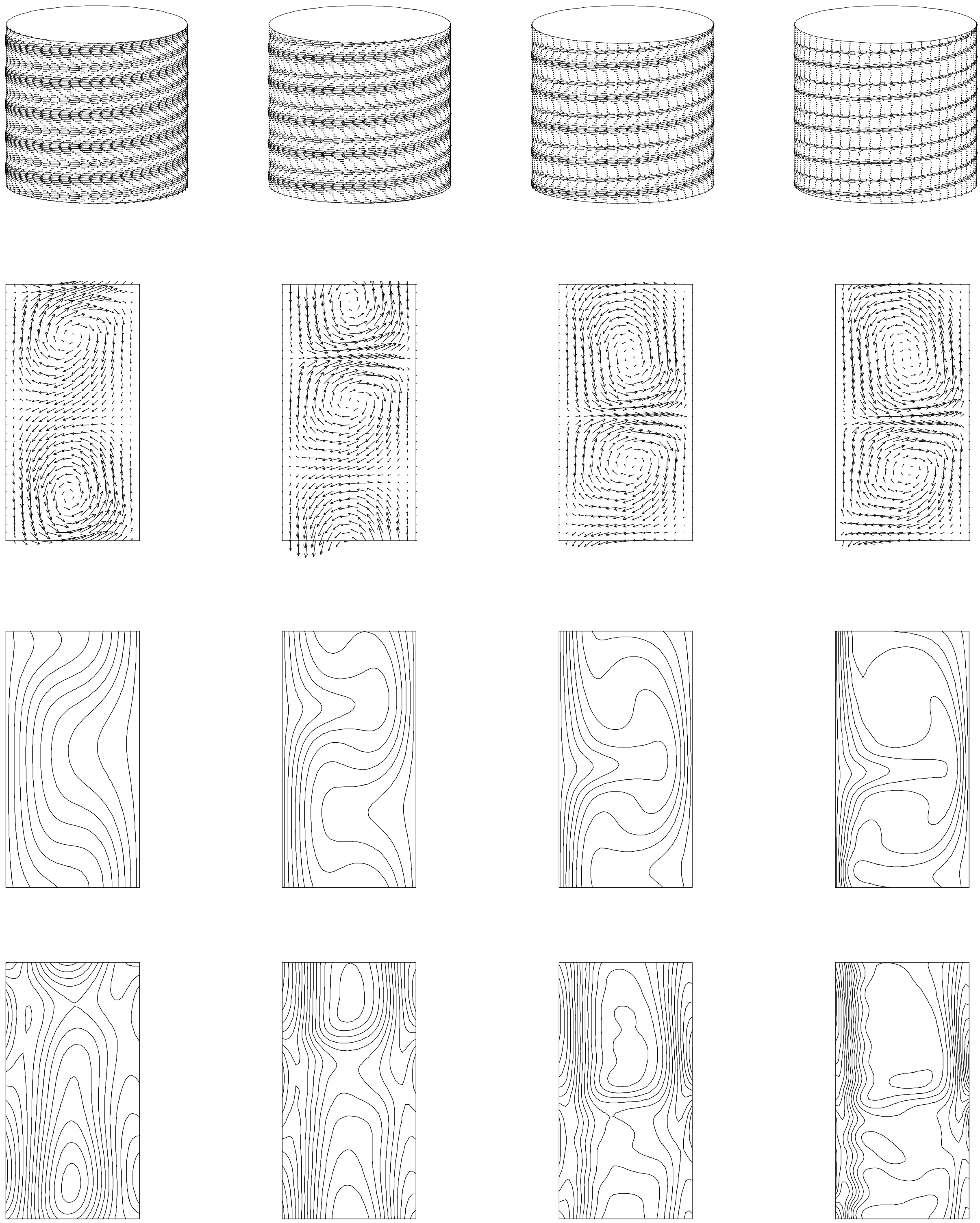

Figure 3: From top to bottom a,b,c,d.

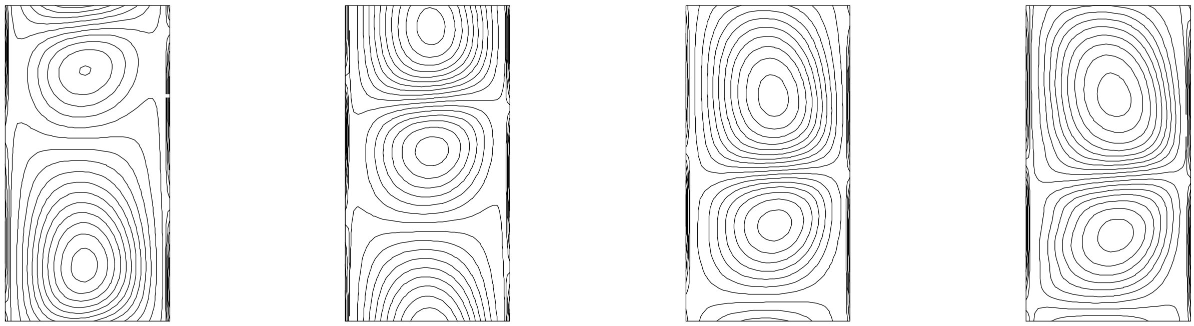

Figure 4:

The boundary conditions say that the radial flux is zero, and this condition guarantees the existence of a stream function $\chi(r, \rho, t)$ such that

$$v_r = -\frac{1}{r}\partial_\rho \chi, \quad v_\rho = \frac{v_z}{b} - \frac{v_\theta}{r} = \frac{1}{r}\partial_r \chi \quad \Rightarrow \quad \frac{d\chi}{dt} = \partial_t \chi \tag{12}$$

But in the rotating frame the velocity field is steady and therefore the stream function does not depend explicitly on time. In this case $d\chi/dt = 0$ and the particle trajectories lie on the surfaces χ =constant. This integral surfaces are invariant by a helical symmetry, and can be obtained from the curves χ =constant in the (r, z) plane (see Figure 4 for the a, b, c, and d aforementioned points) by a helical movement. In the initial non–rotating reference frame these integral surfaces also exist, but they are not steady and they are rotating around the z-axis with frequency Ω.

The stream function has a very simple expression in terms of the velocity potentials:

$$\chi(r, \rho) = \psi - \frac{r}{b}\phi_r + H(r), \quad H(r) = \int_{r_i}^{r} \left(\frac{r}{b}\overline{v}_z - \overline{v}_\theta\right) dr \tag{13}$$

The contribution of the mean flows isin the H term.

A detailed description of the particle trajectories can be obtained from the stream function. The (r, ρ) coordinates of a particle trajectory are periodic in time, the period being the time taken to go over a χ-constant curve. But in a period, the z coordinate may not recover their initial value, undergoing a shift both in the axial and azimuthal directions.

This axial shift per unit time is showed in Figure 5. We notice that the center of the vortices is at rest, and that the axial motion takes place in the boundary layers near the walls and between the vortices. In fact, the previous pictures showed that the stream function has two saddle points near the walls. Surprisingly, the axial motion is confined mainly between the homoclinic curves joining the saddle points, and also near the walls. The shape of these curves can be seen in Figure 6 for the a, b, c cases.

Another striking fact is that these curves tend to merge when the Reynolds number increases. In fact for the point c they are almost identical. Therefore the axial motion concentrates in an internal boundary layer that becomes very narrow at high Reynolds number. Anyway this axial motion is very small compared with the azimuthal velocities of the flow. Figure 7,8 and 9 show the particle paths corresponding to the case a in three different regions. Figure 7 corresponds to an initial point near the outer wall, Figure 8 has the particle path confined between the homoclinic curves, and Figure 9 shows a trajectory of a particle inside the big vortex.

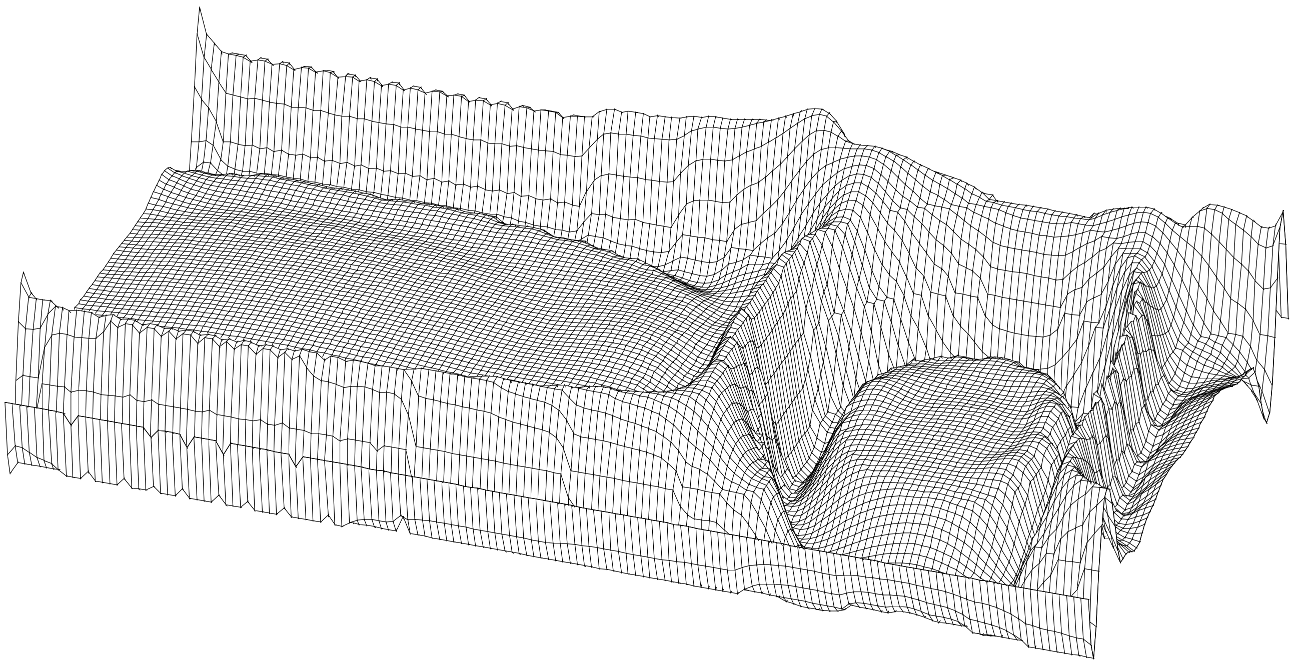

Figure 5: Axial shift per unit time corresponding to the case a. The horizontal coordinates are (r,z).

5 Secondary instabilities.

The results on instabilities and secondary bifurcations we have obtained are a byproduct of the continuation method used. The jacobian matrix of the steady equations is computed during the process, and its eigenvalues tells us if the spiral flow is stable in front of perturbations which do not change the helical symmetry of the flow. Therefore, these special kind of instabilities can be easily examined.

The results shown in Figure 10 say that just before the point a a Hopf bifurcation happens and after, a real eigenvalues crosses the imaginary axis, on the black points in the diagram. Figure 11 shows the Reynolds number corresponding to this secondary Hopf bifurcation as a function of the slope b of the spiral pattern. We have also plotted the curve corresponding to the linear stability of the basic Couette flow. This instability mechanism gives rise to a quasiperiodic motion.

This motion reminds us of a similar phenomena we have obtained before [6], when we computed the evolution in time of a spiral near a bicritical point, where two spirals of the same slope but different number of vortices appear in the first instability. After the bifurcation point, we got a periodic solution corresponding to one of the mentioned spirals. But increasing the Reynolds number, a Hopf bifurcation appeared, and we got a quasiperiodic regime with two frequencies. This quasiperiodic flow showed the competition between the two spirals mentioned before. The flow alternates in time between a spiral with two vortices and another one with four vortices.

6 Conclusions and perspectives.

We have seen that different instability mechanism appear even though we have only considered perturbations that preserve the helical symmetry. Between these instability mechanisms we expect to found

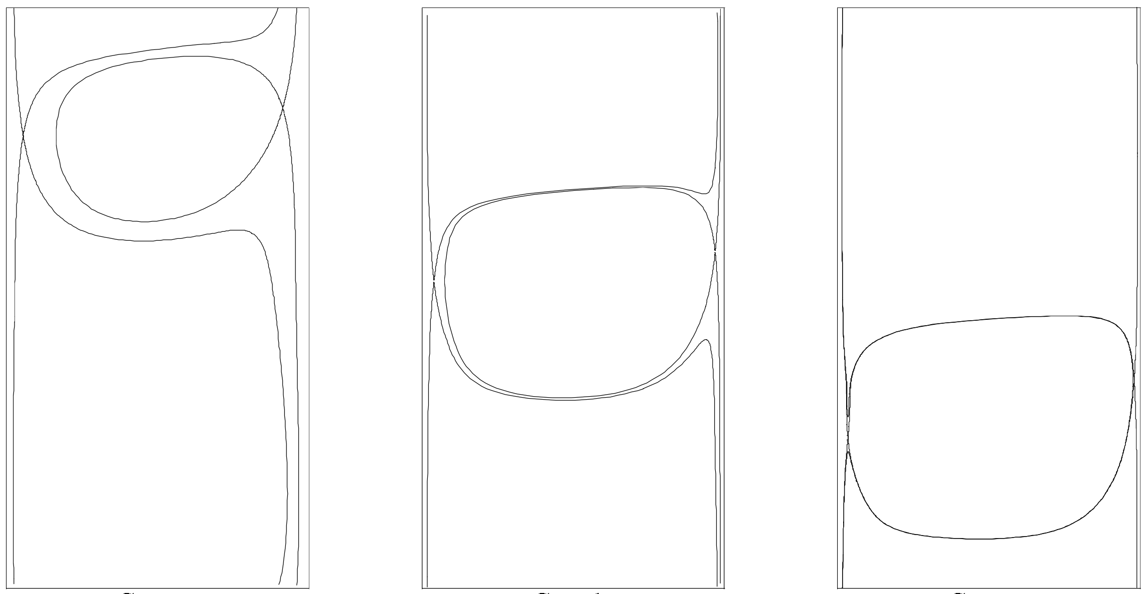

Case a. Case b. Case c.

Figure 6: Homoclinic trajectories of the stream function in a θ-constant plane.

competition between different spiral modes, and also the Eckhaus phenomena, but more numerical work is needed.

Experimental evidence [1], [2] suggest that the dominant bifurcations are fully three-dimensional, and therefore can not be found with the partial stability analysis we have done. Our aim is to carry out a complete linear stability analysis of the spiral flow, including perturbations which break the helical symmetry, in order to obtain the stability balloon of the spiral flow. This work is already in progress.

References

[1] C.D. Andereck, R. Dickman and H.L. Swinney 1983 'New flows in a circular Couette system with co-rotating cylinders.' *Phys. Fluids* **26**, 1395-1401

[2] C.D. Andereck, S.S. Liu, H.L. Swinney. 1986 'Flow regimes in a circular Couette system with independently rotating cylinders.' *J. Fluid Mechanics* **vol. 164**, 155-183

[3] F. Marquès. 1990 'On boundary condition for velocity potentials in confined flows: Application to Couette flow.' *Phys. Fluids A* **2**, 729-737

[4] F. Marquès, M. Net, J. Massaguer and I. Mercader. 1993 'Thermal convection in vertical cylinders. A method based on potentials of velocity.' *Computer Meths Appl Mech Engng* **110**, 157-169

[5] H. Fasel, O. Booz. 1984 'Numerical investigation of supercritical Taylor-vortex flow for a wide gap.' *J. Fluid Mechanics* **138**, 21-52

[6] J. Snchez, D. Crespo, F. Marqus 1993 'Spiral vortices between concentric cylinders.' *Applied Scientific Research*, **51**, 55-59

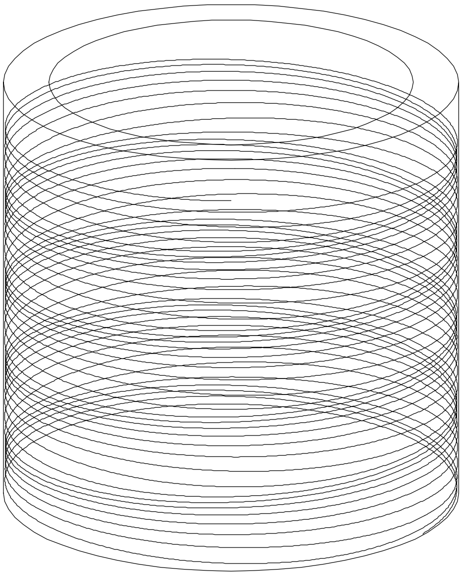

V e l o / c n t r = 1 . 0 0 0 / C f = 1

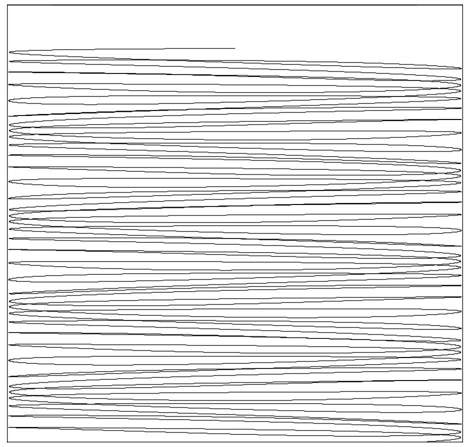

V e l o / c n t r = 1 . 0 0 0 / C f = 1

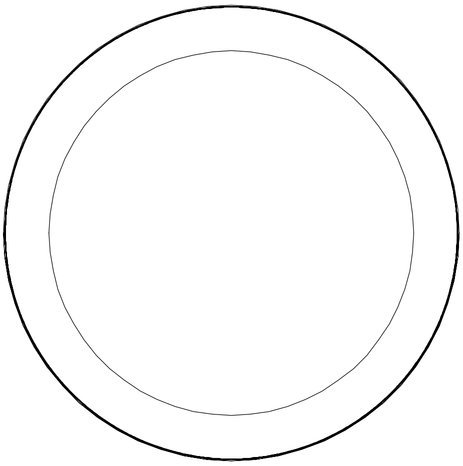

V e l o / c n t r = 1 . 0 0 0 / C f = 1

Figure 7:

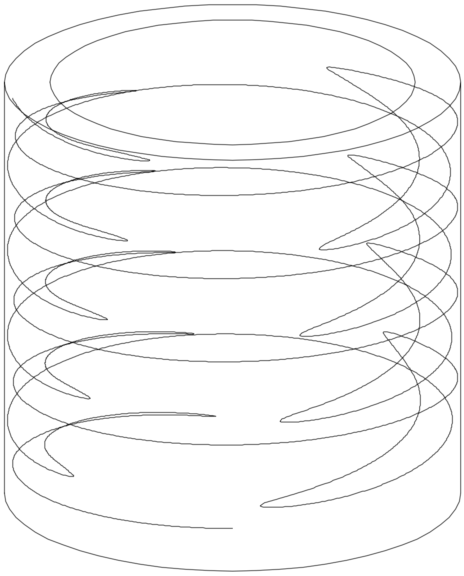

V e l o / c n t r = 1 . 0 0 0 / C f = 1

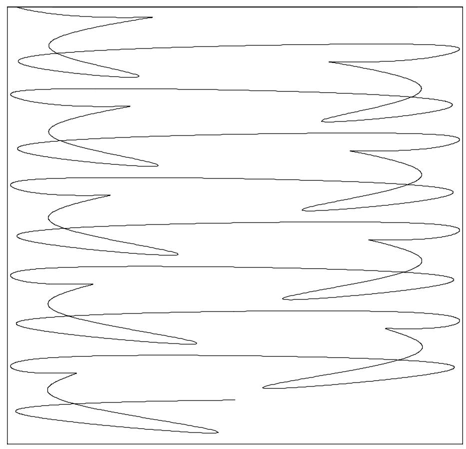

V e l o / c n t r = 1 . 0 0 0 / C f = 1

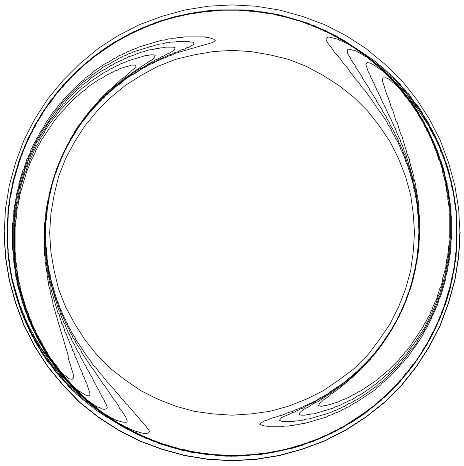

V e l o / c n t r = 1 . 0 0 0 / C f = 1

Figure 8:

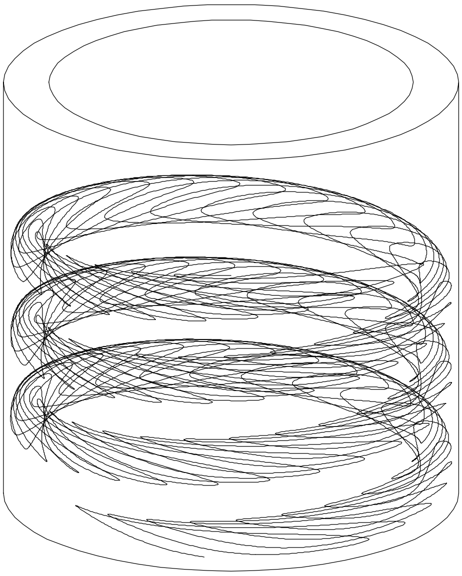

V e l o / c n t r = 1 . 0 0 0 / C f = 1

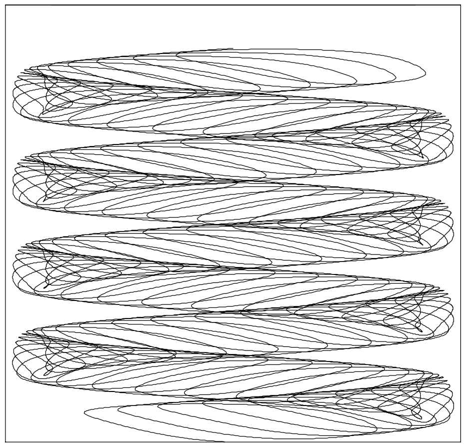

V e l o / c n t r = 1 . 0 0 0 / C f = 1

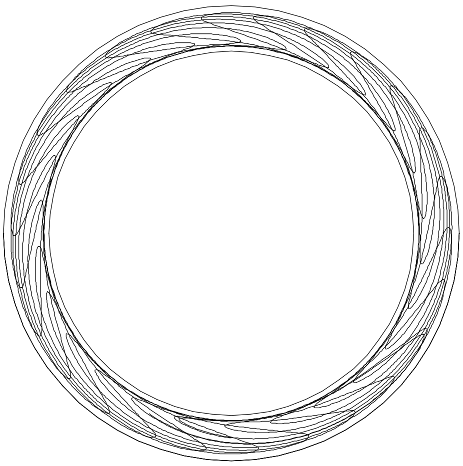

V e l o / c n t r = 1 . 0 0 0 / C f = 1

Figure 9:

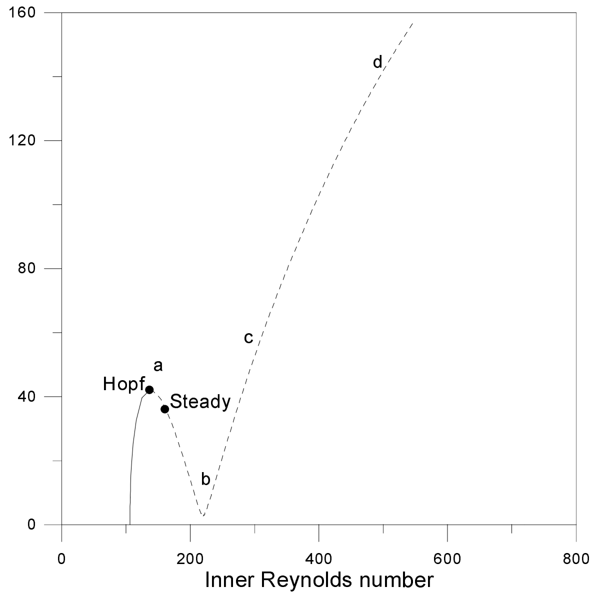

Figure 10: Bifurcations on the spiral branch. The parameter values are the same as in Figure 1.

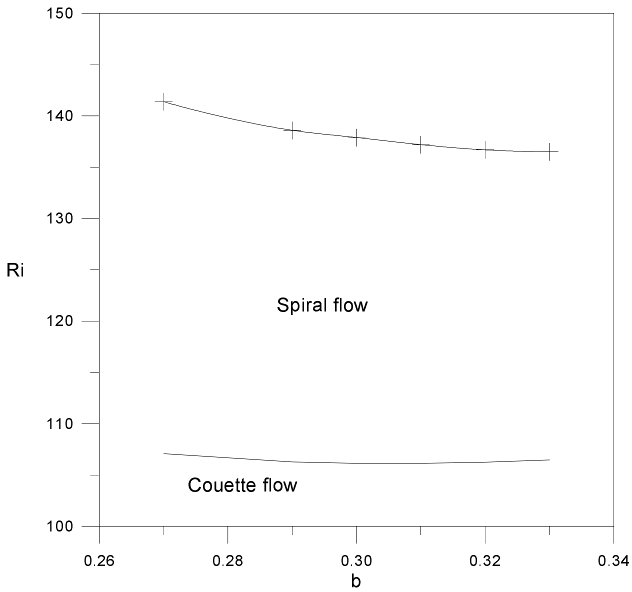

Figure 11: Stability boundaries of the spiral flow. The parameter values are the same as in Figure 1.